Electronic Supplementary Material (ESI) for Environmental Science: Nano.

Supporting Information

Cobalt Ferrite Nanozyme for Efficient Symbiotic Nitrogen Fixation *via* Regulating Reactive Oxygen Metabolism

Jun Ma[a, †], Zhiyong Song[b †], Jianhong Yang[b], Youning Wang[c] & Heyou Han[a,b,*]

[a]State Key Laboratory of Agricultural Microbiology, College of Life Science and Technology, Huazhong Agricultural University, No. 1 Shizishan Street, Hongshan District, Wuhan, Hubei 430070, China.

[b]State Key Laboratory of Agricultural Microbiology, College of Science, Huazhong Agricultural University, No. 1 Shizishan Street, Hongshan District, Wuhan, Hubei 430070, China.

[c]State Key Laboratory of Agricultural Microbiology, College of Plant Science and Technology, Huazhong Agricultural University, No. 1 Shizishan Street, Hongshan District, Wuhan 430070, China.

[†]These authors contributed equally: Jun Ma, Zhiyong Song. *email: hyhan@mail.hzau.edu.cn

1. Materials and methods

Experiment S1. Preparation of iron/cobalt-based materials.

$CoFe_2O_4$-NPs (Purity: 99.5%, APS: 50 nm, SSA:43.34 m^2 g^{-1}) was purchased from Nanjing Emperor Nano Material Co., Ltd. (China). $NiFe_2O_4$-NPs (Purity: 98.0%, APS: 20-30 nm, SSA: 84.76 m^2 g^{-1}), Co_3O_4-NPs (Purity: 99.5%, APS: 30 nm, SSA:11.65 m^2 g^{-1}) and Fe_2O_3-NPs (Purity: 98.0%, APS: 50 nm, SSA:37.04m^2 g^{-1}) were purchased from Aladdin Reagent Co., Ltd.

(Shanghai, China). $CoCl_2$ (analytical purity) was purchased from Sinopharm Chemical Reagent Co., Ltd. (Shanghai, China).

In the initial and directional screening of materials, different cobalt-based materials ($CoFe_2O_4$ nanozyme, $NiFe_2O_4$-NPs, Co_3O_4-NPs, and $CoCl_2$,) were weighed accurately and prepared with ultrapure water at a concentration of 1000 mg L^{-1} ($CoFe_2O_4$ nanozyme, $NiFe_2O_4$-NPs, and Co_3O_4-NPs) and 553.33 mg L^{-1} ($CoCl_2$), which were defined as the mother liquor, and the nano materials were all obtained by 30 min sonication in a sonicator bath (L10-300A) at 40 kHz and 300W. Before use for plant experiments, the directional screening was adjusted to concentrations(1, 10, 100, 500, and 1000 mg mL^{-1}) and $CoCl_2$(0.55, 5.53, 55.33, 276.67, 553.33 mg L^{-1}). Finally, the $CoFe_2O_4$ nanozyme was characterized by transmission electron miscroscopy (TEM), scanning electron microscopy (SEM), atomic force microscopy (AFM), X-ray powder diffraction (XRD), X-ray photoelectron spectroscopy (XPS) and Fourier transform infrared (FTIR) spectroscopy. The related experimental results are shown in Fig. 1.

Experiment S2: Microscopy

The nodular sections for transmission electron microscopy (TEM) and optical microscopy were prepared as previously described.[1] Ultra-thin sections for TEM were sliced using a Leica UC6 ultramicrotome as the tracer of nanomaterials and statistics of the number of rhizobia and semi-thin nodular sections for optical microscopy using a Microm HM360 for observation of cell morphology and staining of internal bacteria. Frozen microtome (Leica CM1950) was used for fluorescent staining to observe the live bacteria in nodules and ROS histochemical localization. Each slice was stained with the mixture of SYTO9 and propidium iodide (PI) stains and held in the dark for 30 min, followed by observation under a fluorescence microscope. The bacteria with intact cell membranes showed green fluorescence, in contrast to red fluorescence for bacteria with damaged membranes.

Experiment S3: Determination of element content.

A certain amount of dried plant tissue powder was accurately weighed, followed by adding 0.5 mL of mixture (hydrochloric acid: nitric acid = 3:1), soaking for 48 h, dilution with 0.5 mL of 1% nitric acid, filtering through a 0.22 micron filter, and 20-fold dilution with 1% nitric acid. Finally, the element content in the digestate was quantified by ICP-MS (Agilent 7900). All the element contents were estimated and converted into element concentrations using data from standard curves (Fig. S2). The element concentration was normalized to the quality ($\mu g.g^{-1}$).

Experiment S4: Determination of nitrogen content

The dried tissue powder (~0.25 g) was weighed into a digestion tube, followed by adding 1mL of H_2O_2, 5 mL of sulfuric acid and 10 drops of perchloric acid to each digestion tube. Next, all the tubes were transferred to a high temperature digestion furnace, heated up to 350°C and held for 1 h. Meanwhile, the solution colour was observed and more perchloric acid was added until the solution was clear. All the digested samples were quantitatively transferred into volumetric flasks and each volume was adjusted to 100 mL with ultrapure water. After dilution to a suitable concentration, a flow analyser (Smart Chem200) was used to detect the nitrogen content, which was converted into nitrogen concentrations using the data from standard curves (Fig. S3). The nitrogen concentrations were normalized to the quality (mg g^{-1}).

Experiment S5. Endogenous ROS detection.

The nodule endogenous H_2O_2 was localized through the reaction of 3,3'-diaminobenzidine (DAB) with H_2O_2 in the presence of endogenous peroxidases to produce a light brown derivative[2] using the staining method as previously reported.[3] The amount of superoxide anion scavenged was detected by measuring the green fluorescent intensity of the cell-permeable fluorogenic dye 2',7'-dichlorofluorescin diacetate (DCFH-DA). Briefly, a certain amount of fresh nodules was weighed into a centrifuge tube, followed by adding DCFH-DA and grinding into homogenate. Finally, the solution was vortexed and centrifuged, followed by measuring the fluorescence intensity. DCFH-DA was excited at 488 nm and emitted at 525 nm.

Experiment S6: Chlorophyll and photosynthesis.

For chlorophyll analysis, the soybean leaves were cut into small pieces with scissors and accurately weighed, followed by extracting the total chlorophyll in 95% ethanol for 24 h. The contents of chlorophyll a and chlorophyll b were measured at 665 nm, 649 nm and 470 nm, and calculated as reported by Porra et al..[4]

$$\text{Chl a}=13.95\times A_{665}-6.88\times A_{649}$$

$$\text{Chl b}=24.96\times A_{649}-7.32\times A_{665}$$

$$\text{Carotenoid}=(1000\times A_{470}-2.05\times \text{Chl a}-114.8\times \text{Chl b})/245$$

Photosynthetic parameter measurement. The net photosynthetic rate was measured at 400 ppm CO_2 partial pressure and irradiances simultaneously with chlorophyll fluorescence using a portable photosynthesis analyser LI-6800 (LI-COR Biosciences， Lincoln, NE) and a fluorometer head 6800-01A (LI-COR Biosciences). Before measurement, leaves were first subjected to light induction for 1 h under steady illumination, an irradiance of 1000 μmol m^{-2} s^{-1}, temperature 28°C, humidity 60%, and flow rate 500 μmol s^{-1}.

Experiment S7: Leghemoglobin content detection

A certain amount of fresh nodules was weighed and homogenized in a phosphate buffer (0.1 mol L^{-1}, pH 6.8) at 4 °C. The amount of phosphate buffer was about 4 times the volume of the nodules. The suspension was centrifuged at 10000 r min^{-1} for 10 min at 4°C to collect the supernatant for measuring the absorbance at 410 nm using a spectrophotometer.

Experiment S8: Dynamic dispersion stability of nanoparticles in matrix

After river sand (1kg) and nanoparticles (100 mg) were uniformly mixed, the nitrogen-free nutrient solution was irrigated every 5 days during the entire sampling process (iron and cobalt were also limited), and the iron and cobalt were sampled separately on day 7, 14, 21, 28, and 35 during the experiment. The detailed method for the leaching level of ions is as follows: each mixed matrix (1 g) was collected at a depth of 3 cm from the surface of the matrix, followed by soaking in 3 ml 1% nitric acid solution for 30 min, shaking 3 times during the process, and

passing through a 0.22 μm filter membrane to collect the filtrate. After 5-fold dilution, the content of iron ion and cobalt ion in the solution was detected by ICP-MS and converted into iron or cobalt ion concentration using the data from standard curves (Fig S4). The element concentration was normalized to the quality ($\mu g.g^{-1}$). Samples treated with $CoFe_2O_4$ nanozyme were collected at day 10, 20, and 30 for scanning electron microscopy mapping to evaluate the dispersion of nanoparticles in the matrix. Iron, cobalt and oxygen were detected separately to accurately trace the distribution of cobalt ferrite.

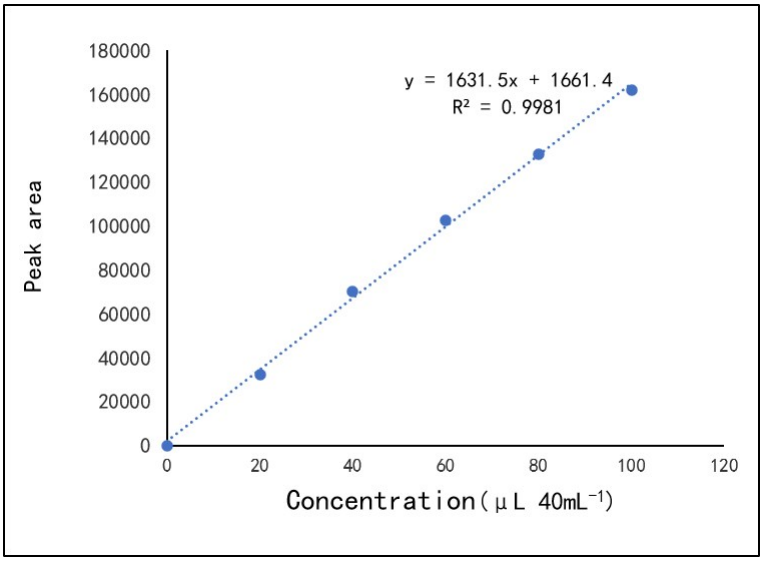

Fig. S1 Standard curve of nitrogenase activity detection.

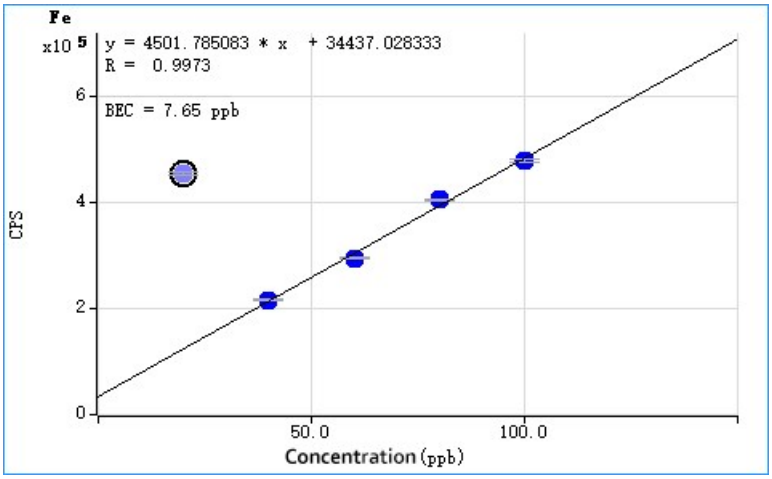

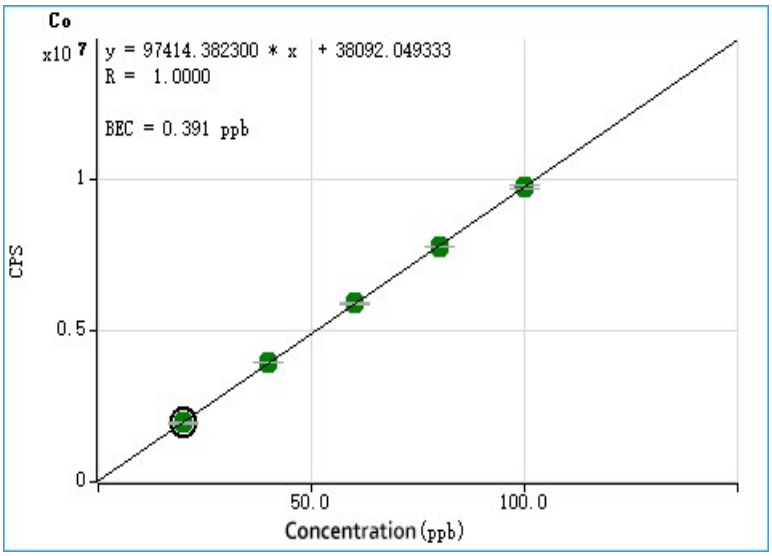

Fig. S2 Standard curve for determinating the element content

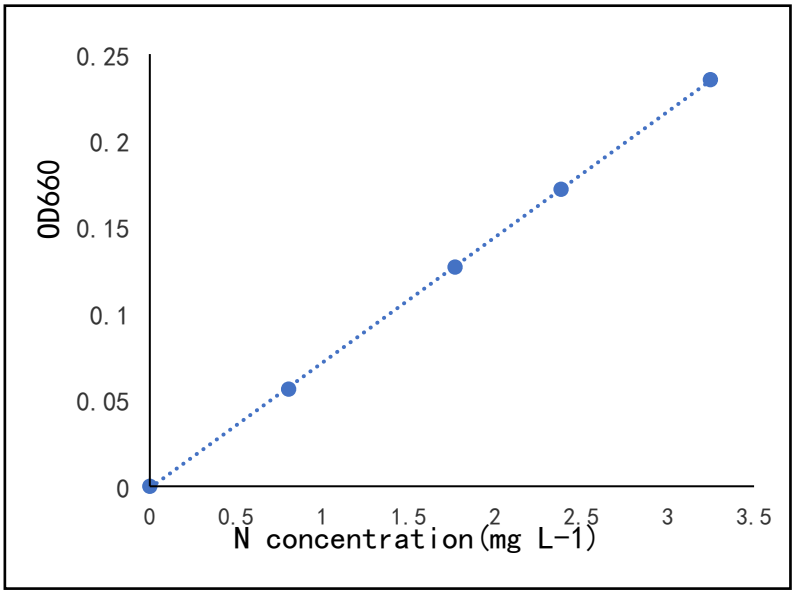

Fig. S3 Standard curve for determinating the total nitrogen

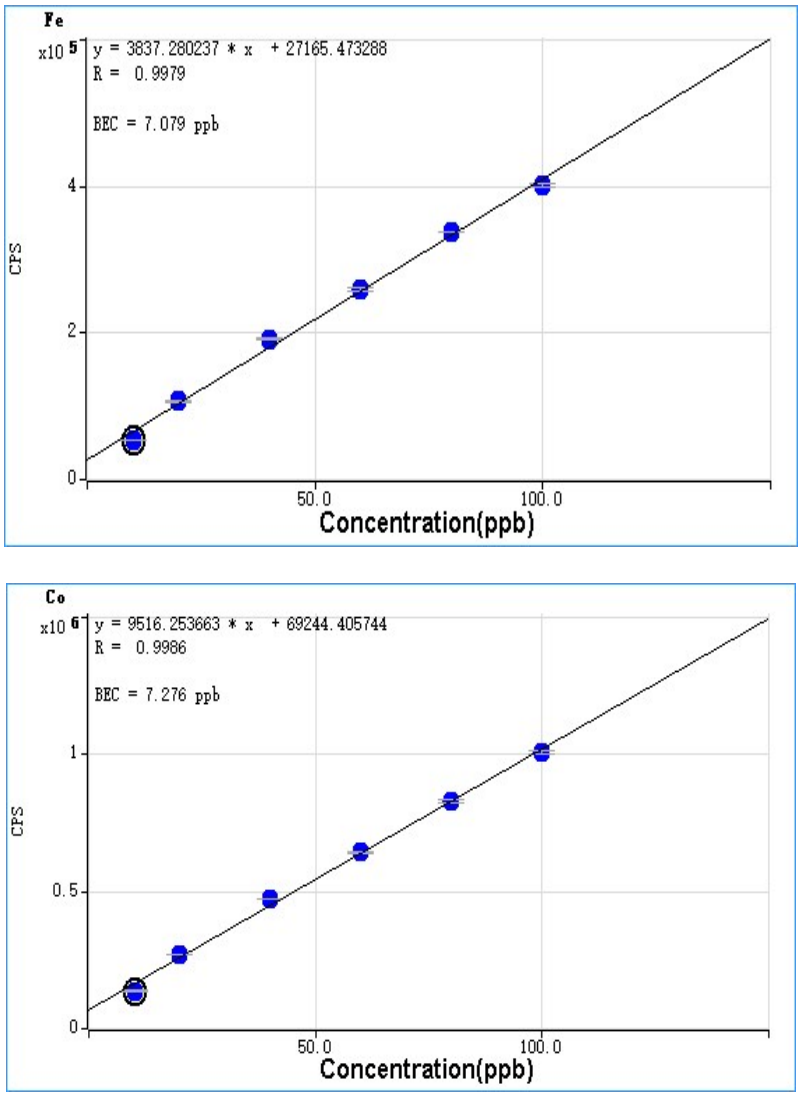

Fig. S4 Standard curve for determinating the element content

2. Results and discussion

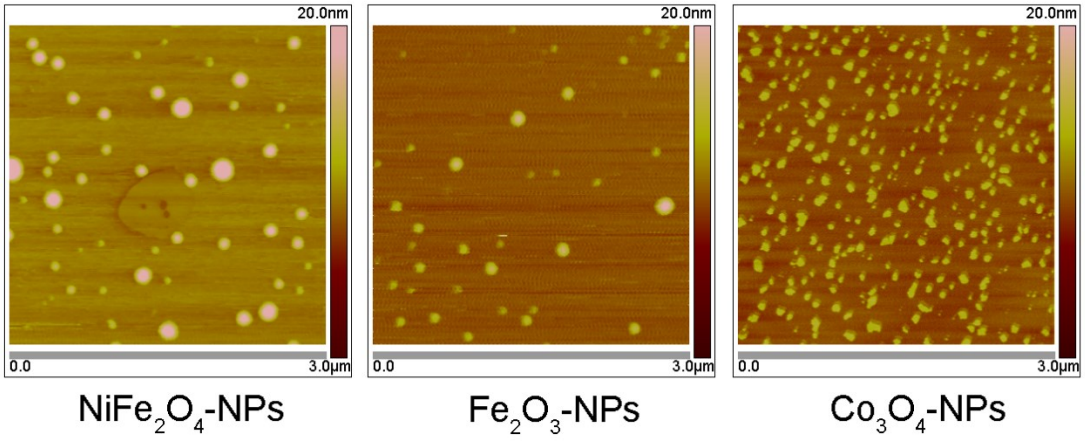

Fig. S5 AFM images of $NiFe_2O_4$-NPs, Fe_2O_3-NPs, and Co_3O_4-NPs

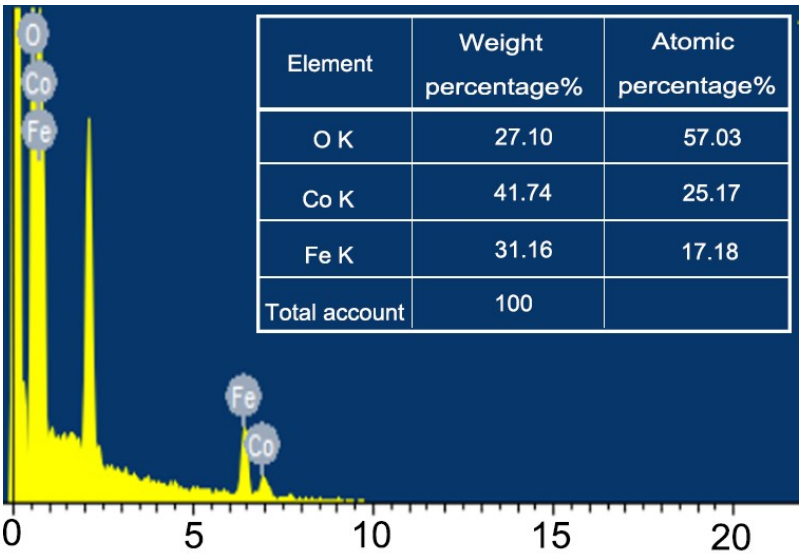

Element	Weight percentage%	Atomic percentage%
O K	27.10	57.03
Co K	41.74	25.17
Fe K	31.16	17.18
Total account	100	

Fig. S6 EDX elemental mapping of $CoFe_2O_4$ nanozyme

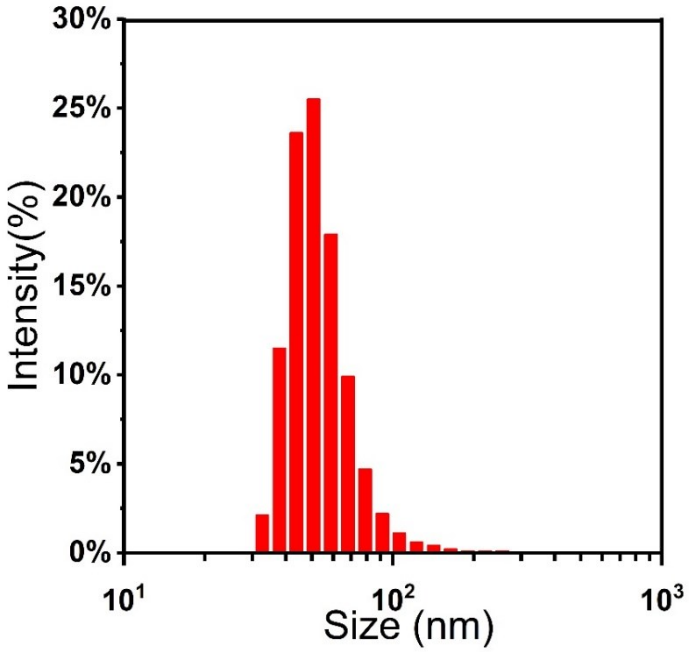

Fig. S7 Hydrodynamic diameter measured in DI water

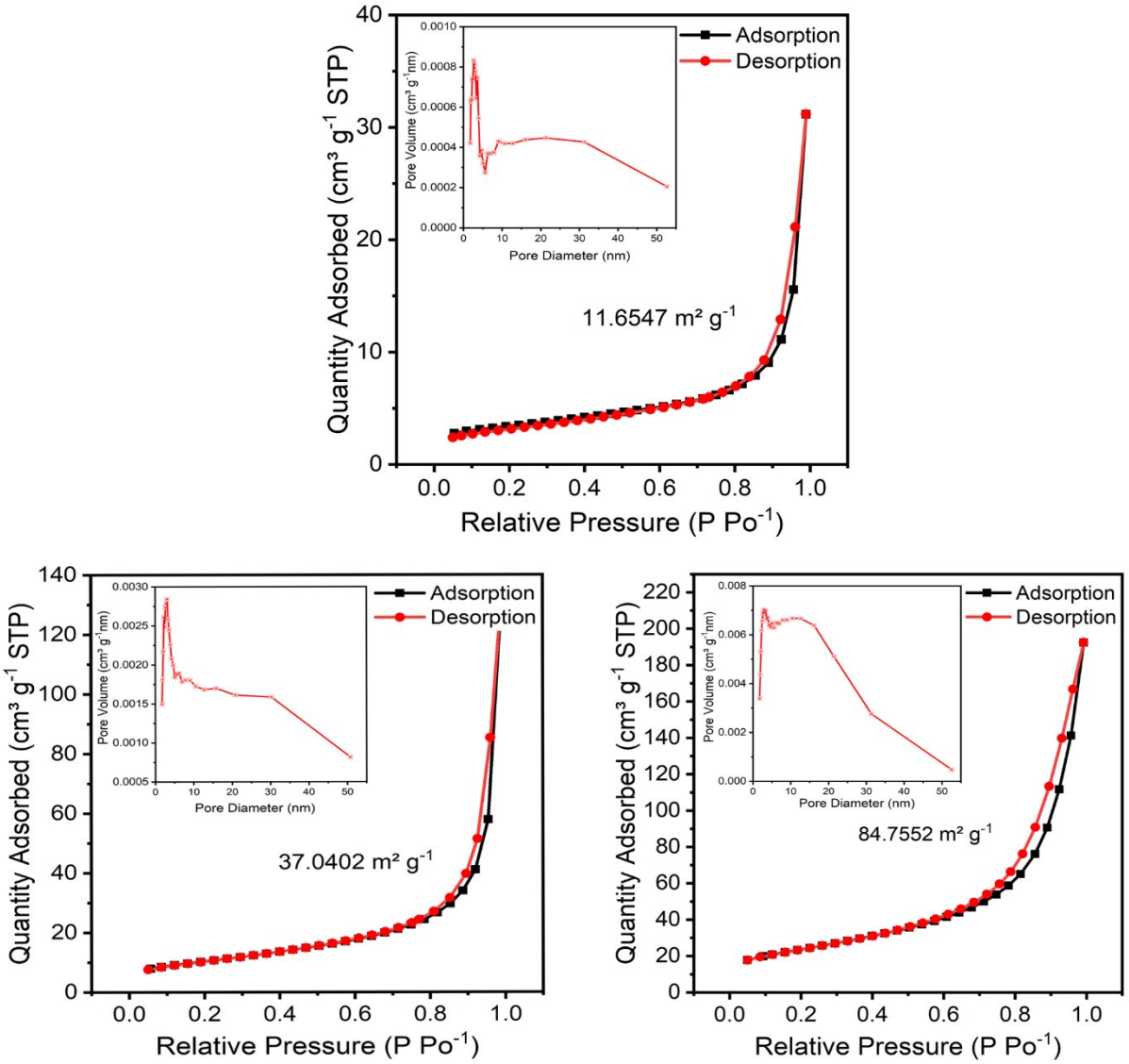

Fig. S8 Nitrogen absorption-desorption isotherms and pore size distribution.

a Co_3O_4-NPs. **b** Fe_2O_3-NPs. **c** $NiFe_2O_4$-NPs

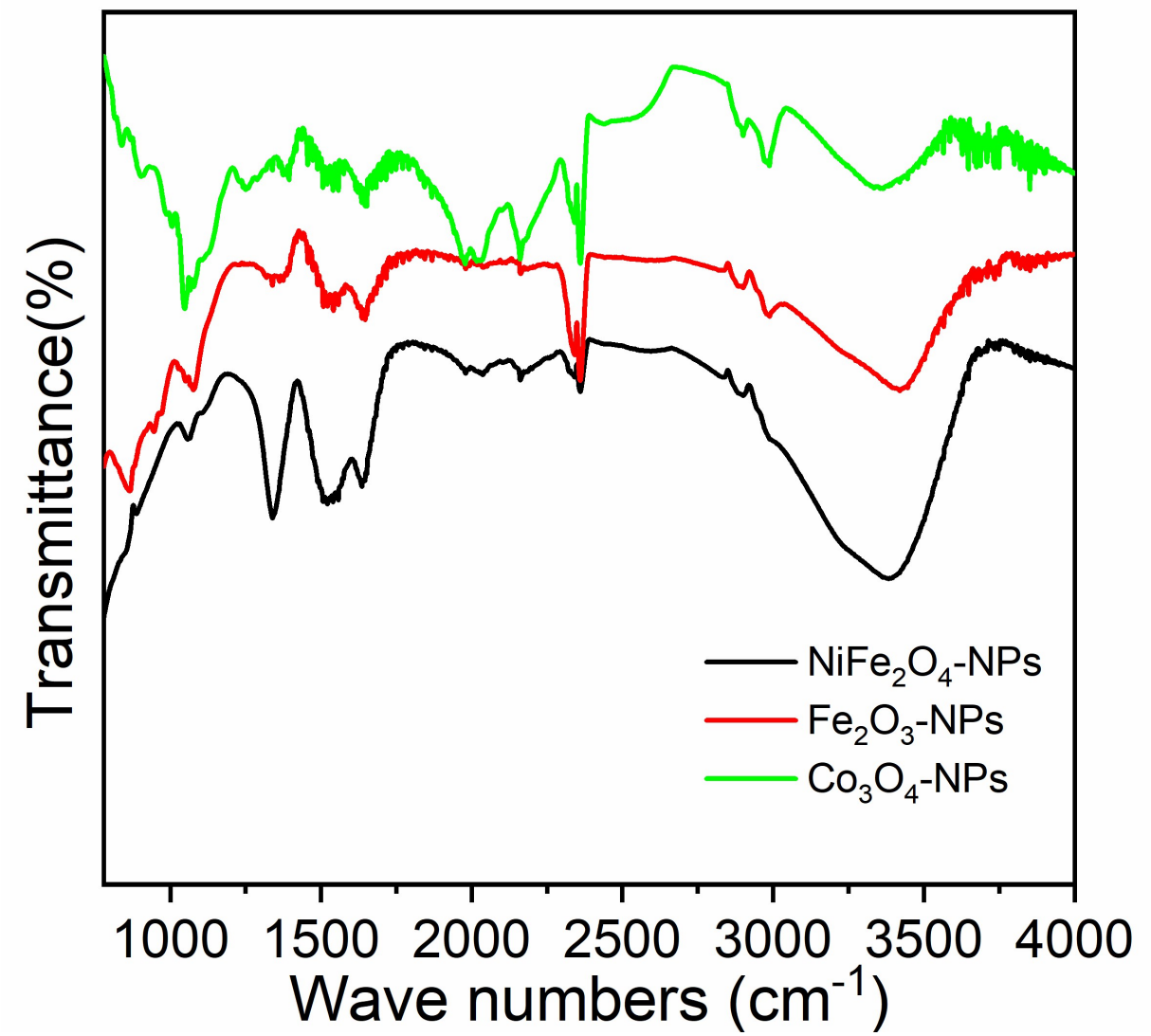

Fig. S9 Fourier transform infrared (FTIR) spectra of $NiFe_2O_4$-NPs, Fe_2O_3-NPs and Co_3O_4-NPs

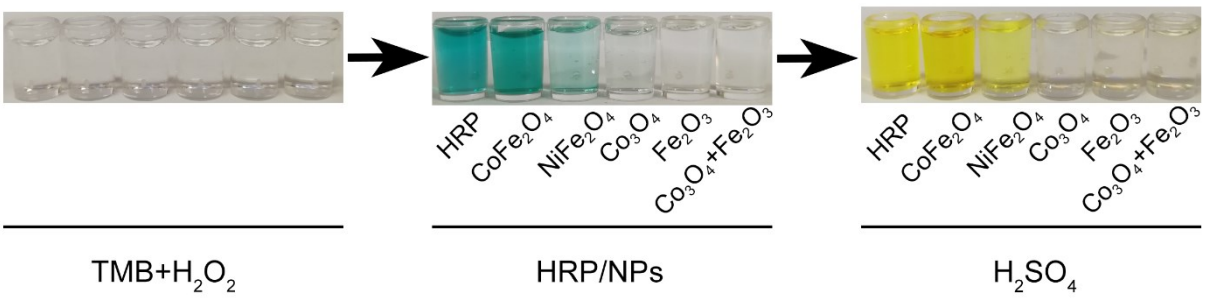

Fig. S10 Verification of NPs catalase activity.

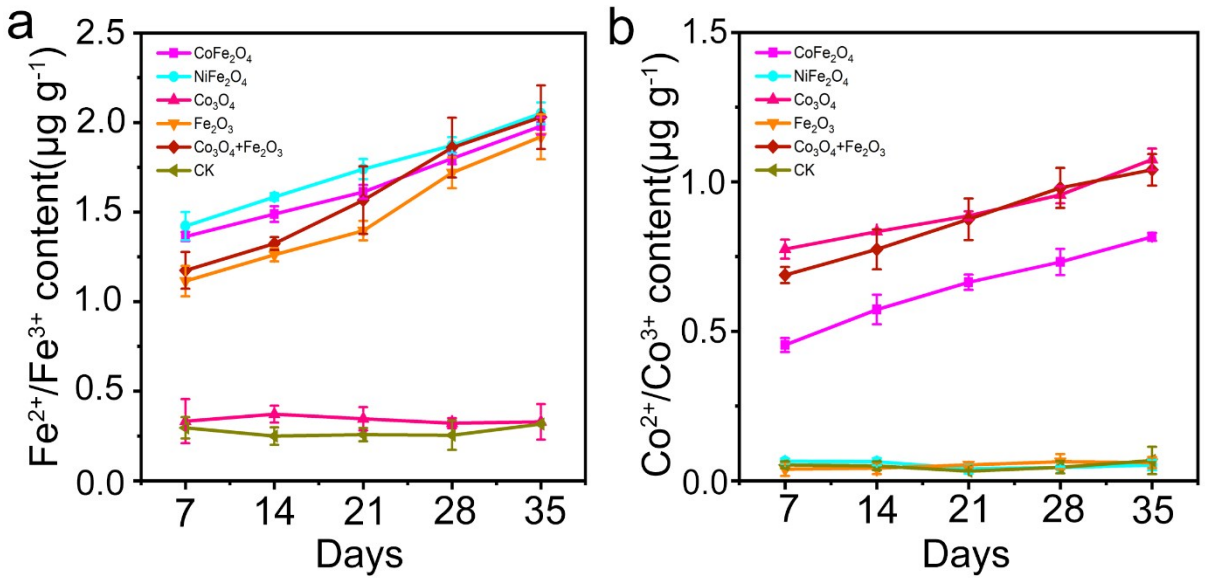

Fig. S11 Kinetic changes of water-soluble iron ions (**a**) and cobalt ions (**b**). (n = 3 technically independent samples; measurements were plotted individually)

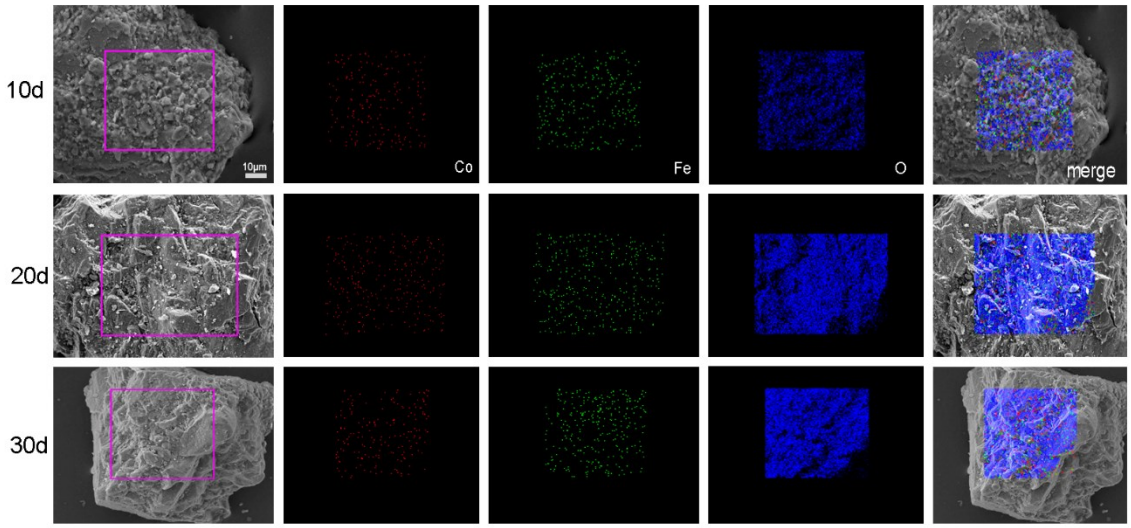

Fig. S12 The dispersion kinetic stability of cobalt ferrite in the matrix. Cobalt (red), iron (green), and oxygen (blue) are uniformly distributed in the matrix.

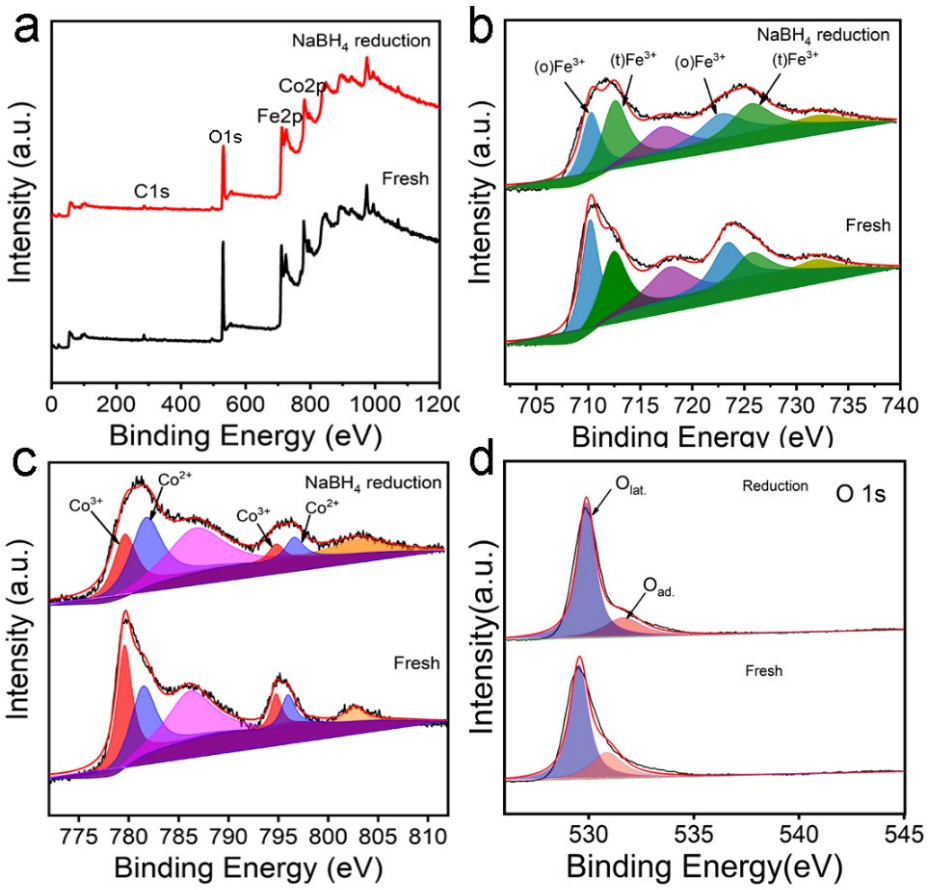

Fig. S13 XPS spectra of the fresh and reacted $CoFe_2O_4$ particles: **a** full-range scan of the samples and **b** Fe2p, **c** Co2p, and **d** O1s core level.

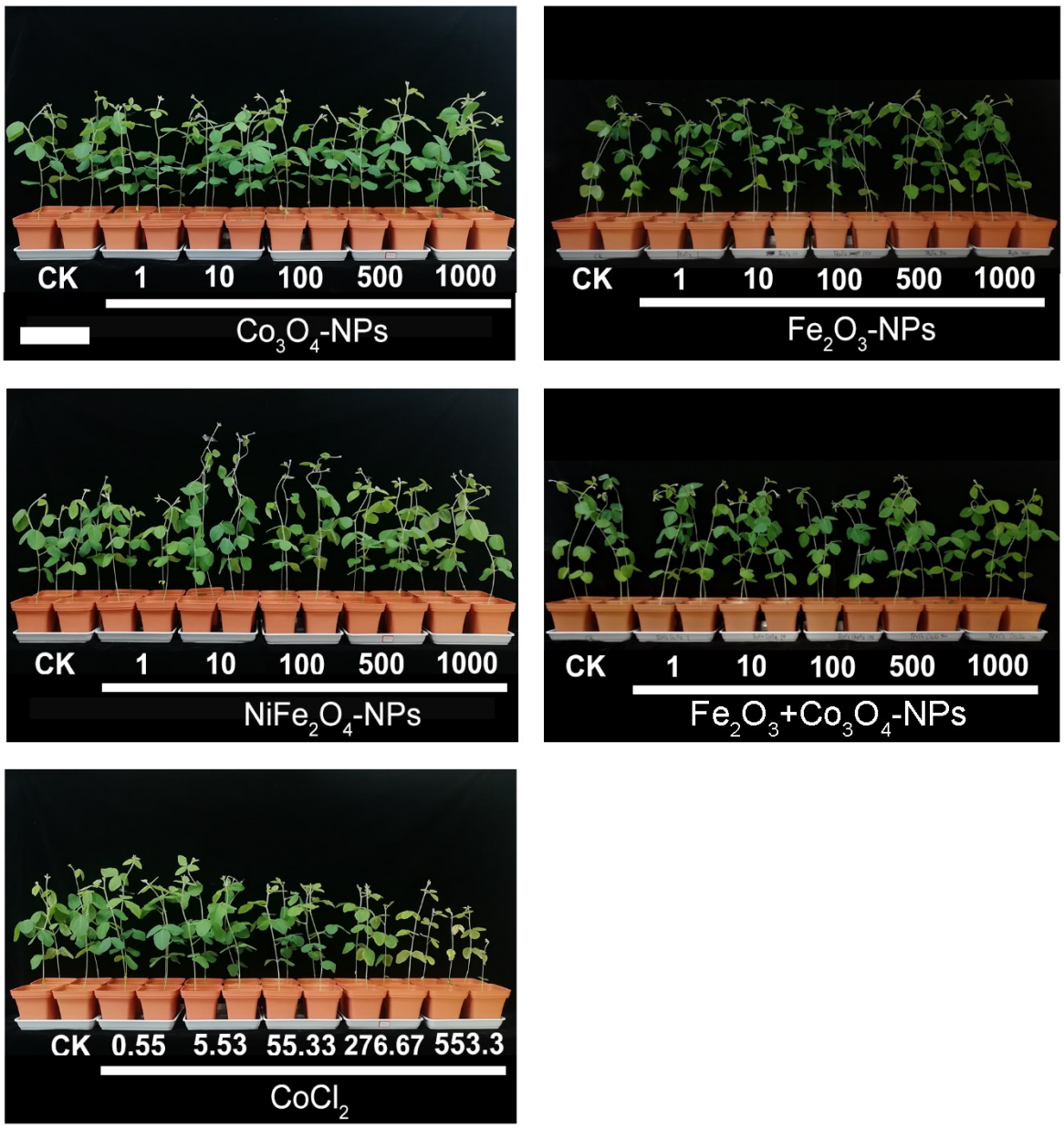

Fig. S14 Phenotypes of soybean plants grown in the soils treated separately with Co_3O_4-NPs, Fe_2O_3-NPs, $NiFe_2O_4$-NPs, Fe_2O_3+Co_3O_4-NPs, and $CoCl_2$ for 28 d. Scale bar=330 mm.

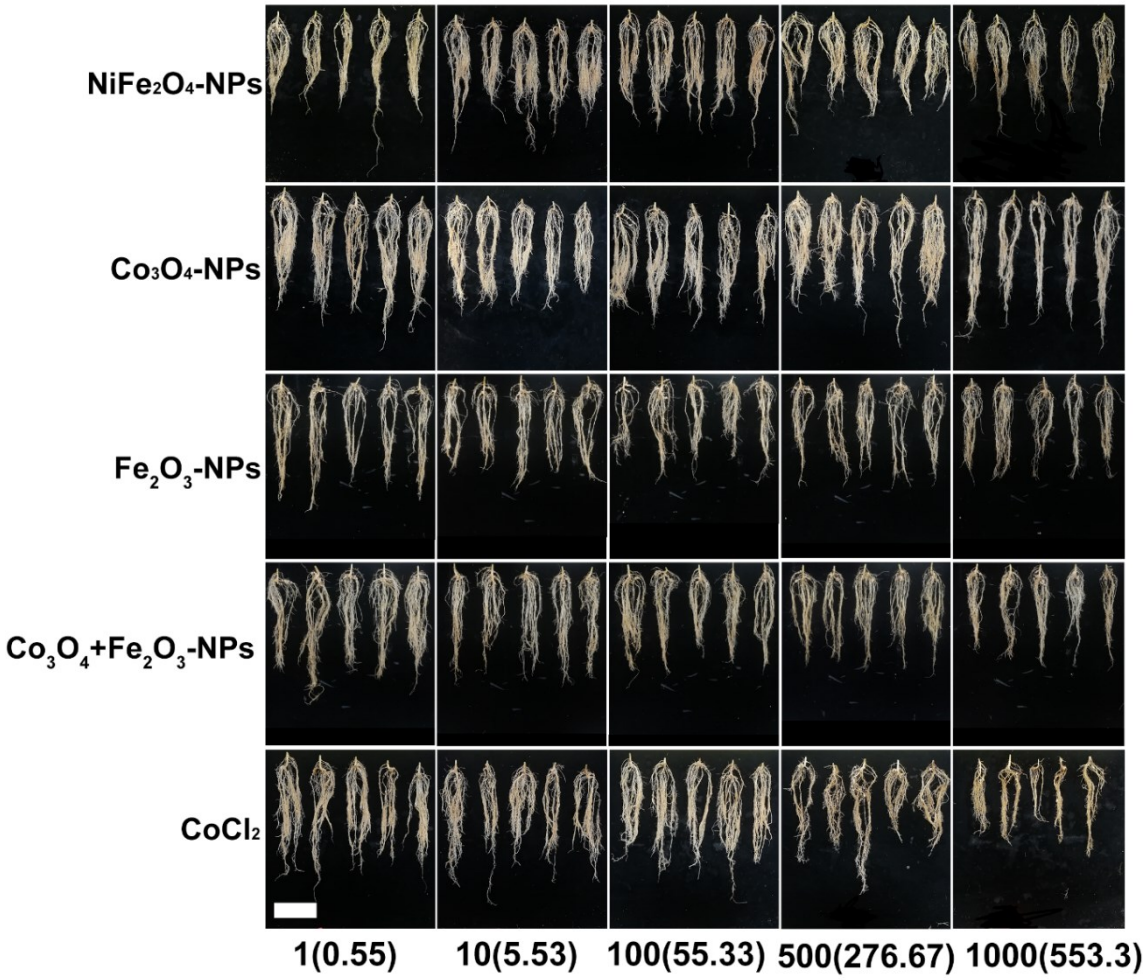

Fig. S15 Root system of soybean treated separately with $NiFe_2O_4$-NPs, Co_3O_4-NPs, Fe_2O_3-NPs, Co_3O_4+Fe_2O_3-NPs and $CoCl_2$ for 28 d. Scale bar=100mm.

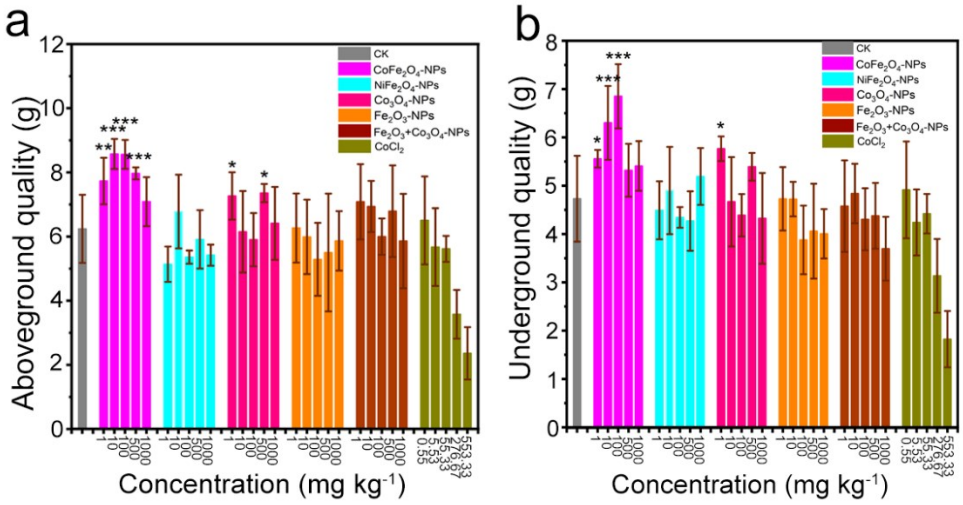

Fig. S16 Effects of different nanomaterials on the growth index of soybeans**. a** Above-ground quality. **b** Underground quality. Results are shown as average ± SE using n = 9 individual plants for each condition. Bars with different asterisks represent significant differences ($p < 0.05$). *$p < 0.05$, **$p < 0.01$, and ***$p < 0.001$ when compared with the control group.

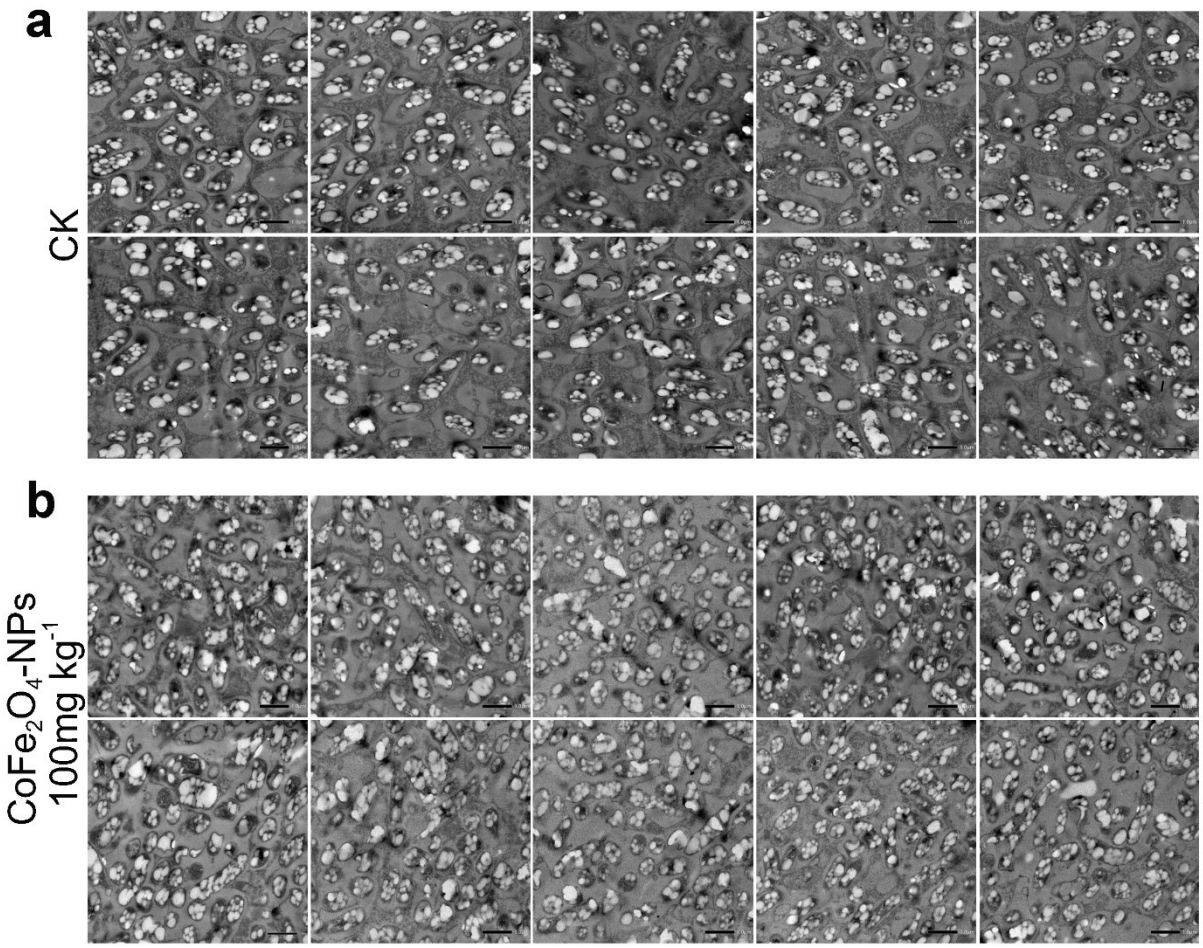

Fig. S17 Comparison of the number of rhizobia in nodules without (**a**) / with (**b**) exposure to $CoFe_2O_4$-NPs-100 mg kg^{-1}.

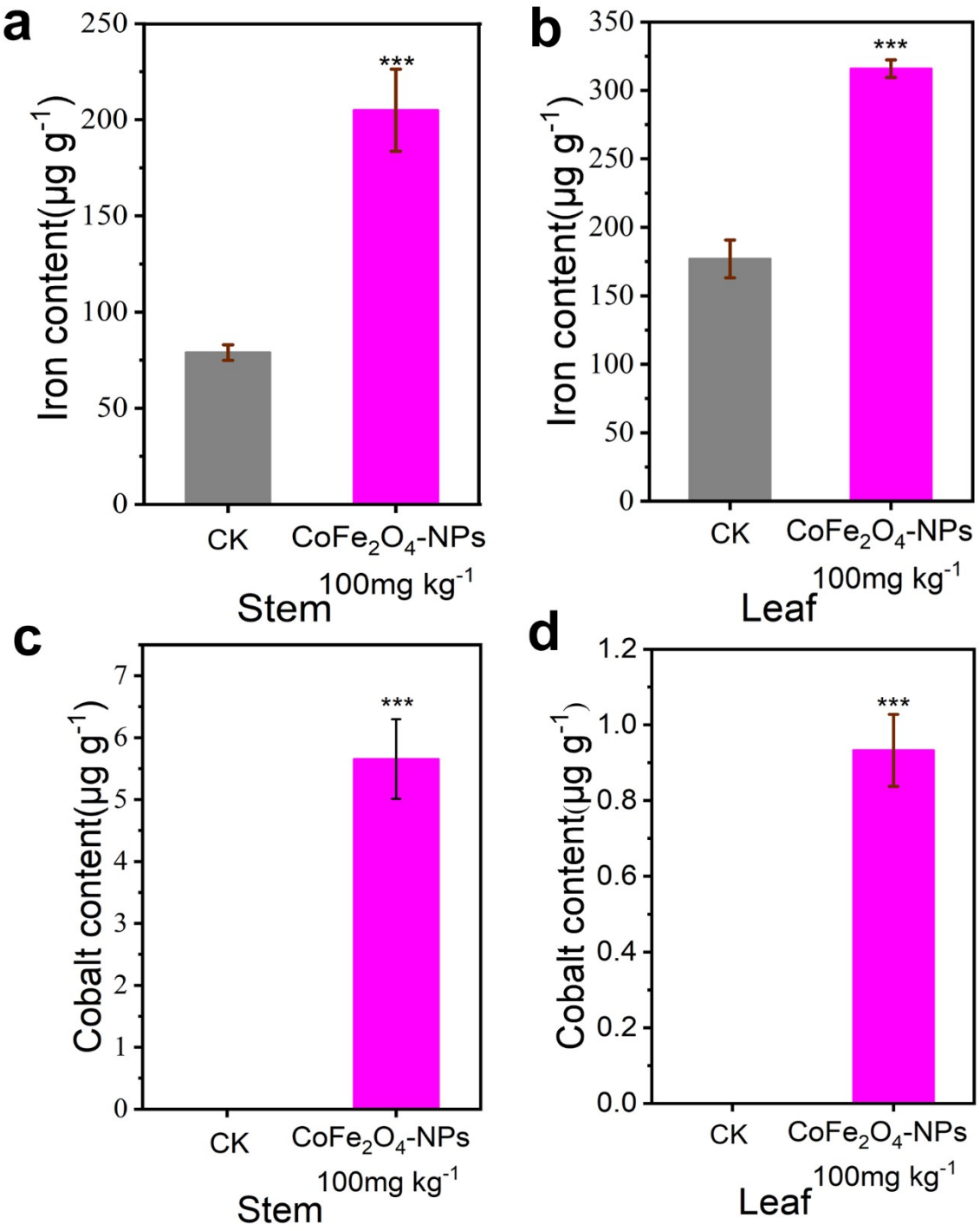

Fig. S18 The iron/cobalt content in the stem or leaf of soybeans with/without exposure to $CoFe_2O_4$-NPs-100mg kg^{-1} for 28 d. **a** Iron content in stems. **b** Iron content in leaves. **c** Cobalt content in stems. **d** Cobalt content in leaves. (n = 3 technically independent samples; measurements were plotted individually).*** indicates significant differences at $P < 0.001$.

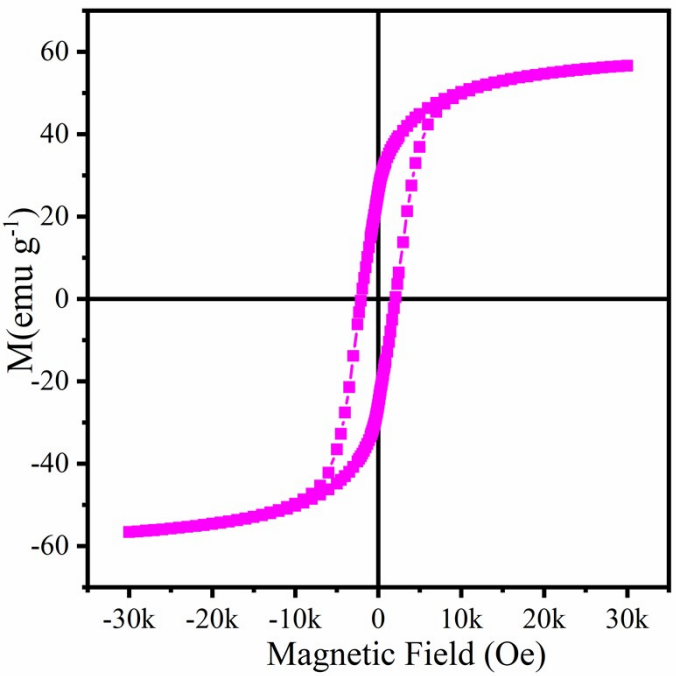

Fig. S19 Hysteresis Loop of $CoFe_2O_4$ nanozyme

Table S1 Primer sequences used in the gene expression analysis.

Ubiquitin	forward	ATGCAGATCTTCGTCAAGACCTTG
	reverse	ACCTCCCCTCAGACGAAG
nifA	forward	ACCAGCCGTGCTCAAAGTG
	reverse	CTGCGTTTATCGGTGTCCC
nifD	forward	AAAGCCAAGGAGCACGAAA
	reverse	ACCACCCGAAGCCCAATCT
nifH	forward	GCTCTATGCCGCCAACAAC
	reverse	TGGATTACCGTCATCTTCCTCA
nifK	forward	AGACGCCTCAGACCAGTTCG
	reverse	TGCGGGTGTTGTAATGCTG

References

1. L. H. Madsen, L. Tirichine, A. Jurkiewicz, J. T. Sullivan, A. B. Heckmann, A. S. Bek, C. W. Ronson, E. K. James and J. Stougaard, The molecular network governing nodule organogenesis and infection in the model legume *Lotus japonicus*, *Nat. Commun.*, 2010, **1**, 10.
2. C. Manzano, M. Pallero-Baena, I. Casimiro, B. De Rybel, B. Orman-Ligeza, G. Van Isterdael, T. Beeckman, X. Draye, P. Casero and J. C. Del Pozo, The Emerging Role of Reactive Oxygen Species Signaling during Lateral Root Development, *Plant Physiol.*, 2014, **165**, 1105-1119.
3. L. Wang, M. C. Rubio, X. Xin, B. Zhang, Q. Fan, Q. Wang, G. Ning, M. Becana and D. Duanmu, CRISPR/Cas9 knockout of leghemoglobin genes in *Lotus* japonicus uncovers their synergistic roles in symbiotic nitrogen fixation, *New Phytol.*, 2019, **224**, 818-832.
4. W. A. T. a. P. E. K. R.J. Porra, Determination of accurate extinction coefficients and simultaneous equations for assaying chlorophylls a and b extracted with four different solvents: verification of the concentration of chlorophyll standards by atomic absorption spectroscopy, *BBA-Bioenergetics.*, 1989, **975**, 384-394.